9

Research Article Open Access

Maha S. Almutairi, S. Muthu, Johanan C. Prasana, B. Chandralekha, Alwah R. Al-Ghamdi, Mohamed I. Attia*

Comprehensive spectroscopic (FT-IR, FT-Raman, ¹H and ¹³C NMR) identification and computational studies on 1-acetyl-1H-indole-2,3-dione

https://doi.org/10.1515/chem-2017-0026 received August 10, 2017; accepted September 20, 2017.

Abstract: Fourier transform infrared (FT-IR) and FT-Raman spectra of 1-acetyl-1*H*-indole-2,3-dione (*N*-acetylisatin) were recorded in the solid phase and analyzed. The molecular geometry, vibrational frequencies, infrared intensities, Raman activities and atomic charges were calculated using density functional theory (DFT/B3LYP) calculations with a standard 6-311++G(d,p) basis set. The fundamental vibrational modes of N-acetylisatin were analyzed and fully assigned with the aid of the recorded FT-IR and FT-Raman spectra. The simulated FT-IR and FT-Raman spectra showed good agreement with the experimental spectra. The stability of the molecule, arising from hyper-conjugative interactions and charge delocalization, was analyzed using natural bond orbital (NBO) analysis. The dipole moment (μ), polarization (α) and hyperpolarization (β) values of *N*-acetylisatin were also computed. The potential energy distribution (PED) was computed for the assignment of unambiguous vibrational fundamental modes. The HOMO and LUMO energy gap illustrated the chemical activity of *N*-acetylisatin. The energy and oscillator strength were calculated by DFT. Gauge-including atomic orbital NMR (1H and 13C) chemical shift calculations were performed and compared

with the experimental values. Thermodynamic properties (heat capacity, entropy and enthalpy) of the compound at different temperatures were also calculated.

Keywords: N-Acetylisatin, FT-IR, FT-Raman, DFT, NBO, HOMO-LUMO

1 Introduction

Isatin (1H-indole-2,3-dione) is an endogenous compound that has been known for about 150 years. It is an attractive substrate in both organic and medicinal chemistry as it constitutes the core structure of many bioactive molecules endowed with diverse biological activities for anticancer [1, 2] antibacterial [3, 4] antifungal [5] anti-HIV [6, 7] and anticonvulsant [8] applications.

The ease of synthetic accessibility of *N*-acetylisatins and their synthetic utility as precursors to prepare bioactive molecules bearing a glyoxylamide scaffold, gave them a respectable attention in different areas of chemistry including medicinal chemistry [9-11]. Ring opening of N-acetylisatin (Figure 1), via attack of its C2-carbonyl group with various amines, gives the corresponding glyoxylamide derivatives which have widespread applications in organic chemistry in addition to their incorporation in numerous biologically active molecules [12-15].

Figure1: Chemical structure of 1-acetyl-1H-indole-2,3-dione (N-acetylisatin).

Pharmaceutical Chemistry, College of Pharmacy, King Saud University, Riyadh 11451, Saudi Arabia; Medicinal and Pharmaceutical Chemistry Department, Pharmaceutical and Drug Industries Research Division, National Research Centre (ID: 60014618), El Bohooth Street, Dokki, Giza 12622, Egypt, E-mail: mattia@ksu.edu.sa

Maha S. Almutairi, Alwah R. Al-Ghamdi: Department of Pharmaceutical Chemistry, College of Pharmacy, King Saud University, Riyadh 11451, Saudi Arabia

S. Muthu: Department of Physics, Arignar Anna Govt Arts College, Cheyyar 604407, India

Johanan C. Prasana, B. Chandralekha: Department of Physics, Madras Christian College, Chennai 600059, India

3 Open Access. © 2017 Maha S. Almutairi et al., published by De Gruyter Open. [DE STAND This work is licensed under the Creative Commons Attribution-NonCommercial-NoDerivatives 4.0 License.

^{*}Corresponding author: Mohamed I. Attia: Department of

To the best of our knowledge, the molecular structure of N-acetylisatin has not previously been investigated via computational approaches. Thus, the current study reports the spectroscopic analysis (FT-IR, FT-Raman and NMR) of N-acetylisatin with the aid of density functional theory (DFT) calculations in order to understand its structural geometry, inter- and intra-molecular interactions and hydrogen bonding. Moreover, the frontier molecular orbitals (HOMO-LUMO) were computed to predict structural changes and reactive sites. Hyperconjugative interactions and charge delocalization in N-acetylisatin were studied using natural bond orbital (NBO) analysis and the potential energy distribution (PED) was computed for the assignment of the unambiguous vibrational fundamental modes of N-acetylisatin. Thermodynamic properties (heat capacity, entropy and enthalpy) were also calculated at different temperatures.

2 Experimental Section

2.1 General

N-Acetylisatin was synthesized according to the literature procedure [16]. The FT-Raman spectrum of N-acetylisatin was recorded in the region of 4000 to 500 cm⁻¹ in pure mode with a Nd:YAG laser of 100 mW with 2 cm⁻¹ resolution on a Bruker RFS 27 at SAIF, IIT, Chennai, India. The FT-IR spectrum was also recorded in the region of 4000 to 500 cm⁻¹ in evacuation mode using the KBr pellet technique with 1 cm⁻¹ resolution on a Perkin Elmer FT-IR spectrophotometer. NMR (1H and ¹³C) spectra (Figures S1 and S2) were measured in DMSOd on a Bruker NMR spectrometer (Ettlingen, Germany) operating at 500 MHz for ¹H and 125.76 MHz for ¹³C at the Research Centre of the College of Pharmacy of King Saud University, Riyadh, Saudi Arabia. Chemical shifts are expressed in δ -values (ppm), relative to TMS as the internal standard.

2.2 Synthesis

Isatin (10 mmol) was suspended in acetic anhydride (10 mL) and the reaction mixture was heated under reflux for four hours. The cooled reaction mixture was filtered and the collected solid was dried under reduced pressure to give N-acetylisatin as yellow solid m.p. 79-81 °C in 85% yield. 1 H-NMR (CDCl $_{3}$): δ (ppm) 2.73 (s, 3H, CH $_{3}$), 7.35 (t,

J = 7.5 Hz, 1H, Ar-H), 7.71 (dd, 1H, J = 1.0, 8.5 Hz, Ar-H), 7.77 (d, J = 7.0 Hz, 1H, Ar-H), 8.40 (d, J = 8.5 Hz, 1H, Ar-H); ¹³C-NMR (CDCl₃): δ (ppm) 26.5 (C14), 118.2 (C4), 119.2 (C8), 125.3 (C6), 126.2, (C5), 138.9 (C7), 148.6 (C9), 157.9 (C2), 169.7 (C12), 180.2 (C3).

2.3 Quantum Chemical Calculations

All quantum chemical density functional calculations, using the Becke three parameter (B3LYP) hybrid DFT level implemented with the standard 6-311++G(d,p) basis set, were carried out using Gaussian 03W [17] to optimize the molecular geometry. The optimized molecular geometry, corresponding to the minimum potential energy surface, was obtained by solving the self-consisting field equation iteratively. For the optimized structure of *N*-acetylisatin, no negative frequency modes were obtained, proving that a true potential energy minimum had been found. We utilized gradient corrected DFT with a threeparameter hybrid function (B3) for the exchange part of the calculations. Whereas, the Lee-Yang-Parr (LYP) correlation function [18] was accepted as an effective approach for the computation of the molecular structure, vibrational frequencies and energies of the optimized structures. By combining the results of the Gauss view program [19] with symmetry considerations, vibrational frequency assignments were made with a high degree of accuracy.

The calculated normal mode vibrational frequencies provided thermodynamic properties by the means of statistical mechanics. To improve the agreement between the predicted and observed frequencies, the computed harmonic frequencies were usually scaled for comparative purposes. The descriptions of the predicted frequencies during the scaling process followed the PED matrix. The vibrational frequency assignment was carried out by combining the results of the Gauss view program, symmetry considerations and the VEDA 4 program [20]. The NBO calculations were performed using the NBO 3.1 program as implemented in the Gaussian 03 package at the DFT/B3LYP level, in order to understand the intramolecular delocalization or hyperconjugation. The NMR (1H and 13C) data was obtained from the DFT method using the 6-311++G(d,p) basis set. Characterization of the excited states and electronic transitions was performed using DFT on the corresponding optimized ground state geometries.

3 Results and Discussion

3.1 Molecular Geometry

The first aim of the computational work was to determine the optimized geometry of N-acetylisatin. The optimized molecular structure of N-acetylisatin, with numbering of the atoms, is shown in Figure 2. The optimized structural parameters such as bond lengths and angles were determined by the B3LYP method with 6-311++G(d,p) as the basis set. The geometry was considered on the basis of C1 point group symmetry.

All calculated geometrical parameters obtained using DFT are in good agreement with the experimental structural parameters [21]. Table 1 summarises the calculated and experimental geometrical parameters of N-acetylisatin. The optimized parameters are slightly different from the experimental ones which might be attributed to the fact that the experimental results are for the solid phase, while our theoretical calculations are for the isolated molecule in the gas phase. The heterocyclic ring is essentially planar, making a dihedral angle of 7.96° with the acetyl moiety. The C(2)-C(3) bond length of 1.583 Å is significantly longer than the expected value for a carbon (sp²)-(sp²) single bond (1.48 Å).

3.2 Vibrational Spectral Analysis

Vibrational spectra are mainly determined by the modes of free molecules observed at higher wavenumbers and the lattice (translational and vibrational) modes in the low wavenumber region. Vibrational spectral assignment was performed for the recorded FT-IR and FT-Raman spectra based on the theoretically predicted wavenumbers by DFT and the results are presented in Table 2. N-Acetylisatin contains 21 atoms and therefore has 57 fundamental modes of vibration. All the vibrations were active in both the IR and Raman spectra. The vibrational band assignments were done on the basis of normal coordinate analysis [22] and the PED. None of the predicted vibrational spectra have imaginary frequencies. Discrepancies were corrected by implementing scaling calculations on the wavenumbers with factors of 0.983 and 0.958 for values below and above 1700 cm⁻¹ above 1700 cm⁻¹, respectively. The selected scaling factors were incorporated according to the SQM procedure using a set of 17 transferable scale factors. The PED was calculated by the VEDA 4 program [20]. The obtained experimental spectra and theoretical FT-IR and FT-Raman spectra of the title molecule are shown in Figures 3 and 4, respectively.

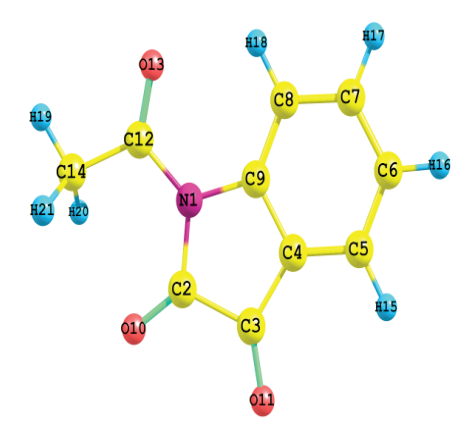


Figure 2: Molecular structure of N-acetylisatin along with numbering of atoms.

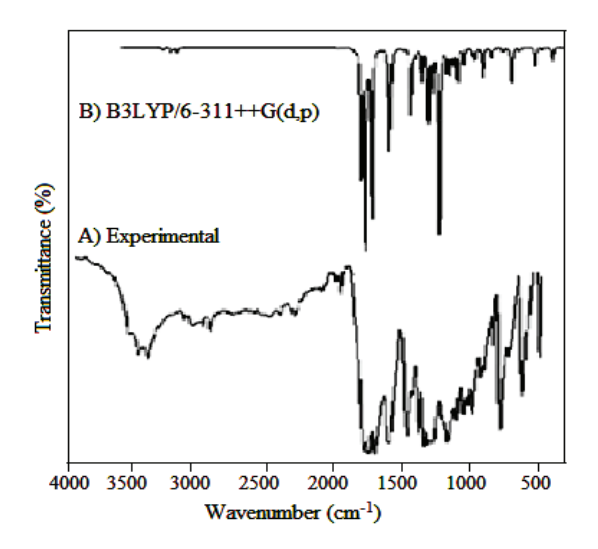


Figure 3: Experimental and calculated FT-IR of N-acetylisatin.

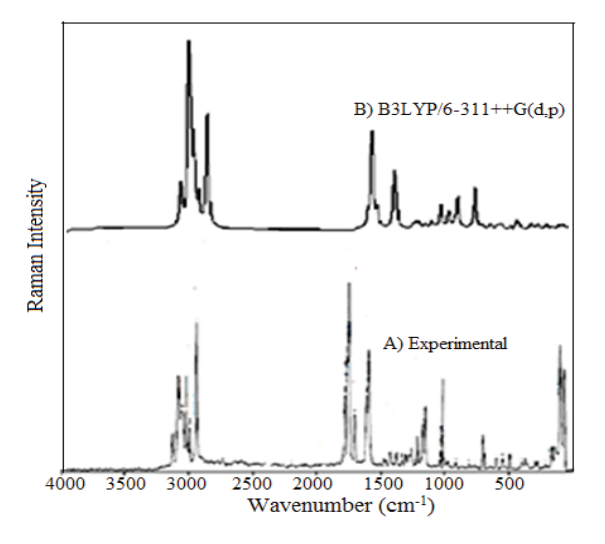


Figure 4: Experimental and calculated FT-Raman spectra of N-acetylisatin.

Table 1: Optimized geometrical parameters bond length, bond angle of the title molecule BYLYP/6-311++G(d,p) in comparison with experimental data.

Bond	Bond angle ()	Bond	Bond length	
	Theoretical values	Experimental values ^a		Theoretical values	Experimental values ^a
C2-N1-C9	108.9	109.3	N1-C2	1.418	1.406
C2-N1-C12	124.8	126.5	N1-C9	1.436	1.434
N1-C2-C3	106.4	106.1	N1-C12	1.421	1.411
N1-C2-O10	128	127.7	C2-C3	1.561	1.538
C9-N1-C12	128	124.2	C2-010	1.199	1.196
N1-C9-C4	110.7	110.5	C3-C4	1.46	1.452
N1-C9-C8	128	129.2	C3-011	1.205	1.205
N1-C12-O13	119	119.7	C4-C5	1.392	1.381
N1-C12-C14	117.6	117.6	C4-C9	1.406	1.383
C3-C2-O10	129.9	126.2	C5-C6	1.391	1.390
C2-C3-C4	108.1	105.1	C5-H15	1.084	1.087
C2-C3-O11	125.6	123.6	C6-C7	1.398	1.389
C4-C3-O11	131.4	131.3	C6-H16	1.083	1.098
C3-C4-C5	129.9	129.5	C7-C8	1.4	1.386
C3-C4-C9	110.8	108.9	C7-H17	1.084	1.079
C5-C4-C9	118.5	121.6	C8-C9	1.39	1.390
C4-C5-C6	118.5	118.5	C8-H18	1.077	1.080
C4-C5-H15	119.8	119.6	C12-O13	1.211	1.220
C4-C9-C8	121.6	120.3	C12-C14	1.507	1.501
C6-C5-H15	122	121.9	C14-H19	1.088	1.086
C5-C6-C7	122.3	119.6	C14-H20	1.091	1.093
C5-C6-H16	120.1	120.4	C14-H21	1.091	1.094
C7-C6-H16	119.8	120			
C6-C7-C8	117.7	122.5			
C6-C7-H17	119.8	119.3			
C8-C7-H17	117.6	118.3			
C7-C8-C9	120.1	117.5			
C7-C8-H18	121.6	121.2			
C9-C8-H18	123.1	121.3			
013-C12-C14	122.3	122.6			
C12-C14-H19	108.9	107			
C12-C14-H20	117.7	111.3			
C12-C14-H21	119.8	111.3			
H19-C14-H20	110.7	110.4			
H19-C14-H21	110.7	110.4			
H20-C14-H21	106.4	106.5			

^a Data was taken from reference [21].

Table 2: Vibrational assignment of fundamental modes of N-acetylisatin along with calculated FT-IR, FT-Raman intensities and normal mode descriptions (characterized by PED) based on quantum mechanical force field calculations using the B3LYP6-311++G(d,p) method.

Mode No.	Mode No. Experimental values		Frequencies IR intensities			Raman activities		Vibrational	
	FT-IR	FT-Raman	Unscaled	Scaled	Relative	Absolute	Relative	Absolute	assignment
1	3130	3130	3260	3123	5	2	1	0	YCH(C10H16, C13H18)(99)
2	3072	3082	3200	3065	9	3	1	0	YCH(C10H16, C13H18) (92)
3		3054	3188	3054	3	1	1	0	YCH (C9H15, C12H17) (99)
4	2972		3176	3042	2	1	1	1	YCH(C9H15, C12H17) (96)
5		3021	3156	3023	8	2	1	0	YCH ₃ (C14H19H20H21)(100)
6	2994	2995	3122	2991	2	1	1	1	YCH ₂ (C14H20H21)(99)
7	2939	2940	3059	2931	1	0	6	3	YCH ₂ (C14H19H20)(100)
8	1782	1781	1840	1763	220	64	5	2	YO ₁₁ C ₃ (82)
9	1751	1759	1810	1734	344	100	0	0	YO ₁₀ C ₂ (77)
10	1711	1704	1770	1696	293	85	0	0	YO ₁₃ C ₁₂ (85)
11	1592	1610	1643	1615	179	52	6	3	YCC(C8-C9, C4-C5) (65)
12		1592	1627	1600	35	10	0	0	YCC(C4-C9, C6-C7) (36)
13	1460	1476	1505	1479	21	6	7	3	YCC(C5-C6) (34)
14	1420	1427	1491	1466	112	33	0	0	βH ₁₈ C ₈ C ₇ (56)
15			1471	1446	12	3	7	3	$\beta H_{15} C_5 C_6 (76)$
16		1410	1456	1431	15	4	7	3	βH19C14H21(78)
17	1376	1379	1407	1383	56	16	11	5	βH20C14H21(48)
18	1334	1334	1362	1339	129	37	0	0	Y(C9-C8, C7-C6) (47),βHCC(13)
19	1306	1307	1333	1310	70	20	1	0	Y(C9-C8, C7-C6)(11))
20	1267	1263	1289	1267	329	96	0	0	YN1C9(47),YC9C12(12)
21	1210	1215	1231	1210	39	11	1	0	Y(C8-C7, C6-C5(40)
22	1163	1172	1208	1187	41	12	0	0	Y(C12-C14(15)
23		1152	1187	1167	28	8	7	3	βH18C8C7(61)
24	1112	1100	1162	1142	57	17	4	2	Υ(C3-C4, C12-C14) (14), βC2C3C4(11)
25	1094	1042	1115	1096	30	9	0	0	YC8C7(11),βH18C8C7(23)
26	1039	1017	1056	1038	5	1	0	0	βH20C14H21(24),τH18C8C9N1(47)
27	1012		1055	1037	11	3	63	27	ΥC7C8(10),βH21C14C12(10),βC2C3C4(17)
28			1032	1015	22	6	1	0	βC9C4C5(24)
29	979	979	1012	995	1	0	0	0	τΗ19C14C11(52),τΗ19C14C11N4 (21)
30		951	983	967	2	1	1	0	τH15C5C4C3(21),τH18C8C9N1(17),τC2C3C 4C9(20)
31	909	930	977	960	52	15	47	20	YN1C9(10),YC12C14(24),βO1C12C14(11)
32		911	915	900	19	6	7	3	YN1C2(11),YC2C3(41)
33	880	862	904	889	1	0	1	1	τH16C6C7(41),τH21C14C12N1(40)
34		831	885	870	4	1	24	10	YN1C2(12),βO10C2C3(41)
35	812	810	832	818	7	2	36	16	opbO11C3C4C9(38),opbC2C3C4C9(11)
36		765	773	760	61	18	3	1	τH15C5C4C3(80)
37	766	740	734	721	1	0	11	5	τC5C6C7C8(65),opbN1C9C8C7(16)
38	705	706	717	705	7	2	7	3	ΥC2C3(23),βC12C13C10(17), βO10C2C3(15)
39		687	699	687	4	1	7	3	ΥC9C4(10),βC9C4C5(28)
40	596	598	603	592	32	9	8	3	τH19C14C12N1(27),opbH19C14C12(44)
41		570	602	592	2	1	6	3	β013C12C14(46),βC4C5C6(17)

230 — Maha S. Almutairi et al.

continued **Table 2**: Vibrational assignment of fundamental modes of *N*-acetylisatin along with calculated FT-IR, FT-Raman intensities and normal mode descriptions (characterized by PED) based on quantum mechanical force field calculations using the B3LYP6-311++G(d,p) method.

Mode No.	o. Experimental values		Frequencies		IR intens	sities	Raman a	ctivities	Vibrational
	FT-IR	FT-Raman	Unscaled	Scaled	Relative	Absolute	Relative	Absolute	assignment
42		551	555	545	4	1	2	1	ΥC5C6(11),βC2C3C4(34)
43	531	530	537	528	0	0	30	13	τC9C5C6C10(10),opbO10C2N1C12(18)
44	495	494	495	486	2	1	81	35	YC5C6(26),βC5C6C7(11),βC14C12N1(11)
45	466	470	476	468	24	7	28	12	opbO11C3C44C5(23), opbN1C2C3C4(15)
46		402	400	393	1	0	147	63	YC5C6C7C8(62),opbO11C3C4C5 (16)
47		380	397	390	1	0	19	8	YN1C2(12),βN1C9C4C3(32),βC14C12N1(25)
48		372	367	360	5	1	174	75	YN1C9(27),βO13C12C14(18),βC14C12N1(26)
49		351	346	340	4	1	44	19	β010C2C3(51)
50		293	289	284	1	0	75	32	τC5C6C7C8(38)
51		276	273	269	5	1	74	32	βΟ10C2C3(25),βC3C4C5(31)
52		215	213	209	9	3	92	40	YC12C14(11),βC12N1C2(61)
53		164	176	173	0	0	233	100	τH18C8C9N1(85)
54			144	142	2	0	63	27	opbO10C2C3C4(11),opbC5C4C9N1(14)
55			108	107	0	0	92	40	τC9C4C5C6(49),opbC5C4C9N1(24)
56			63	62	0	0	233	100	τC9C8C7C6(38)
57			50	49	8	2	63	27	τC14C12N1C9(70)

Y: stretching; β : bending; τ : torsion; opb: out of plane bending; Relative absorption intensities normalized with highest peak absorption equal to 100; Relative Raman intensities normalized to100; scaling factor 0.958 for the wavenumbers above 1700 cm⁻¹ and 0.983 for the wavenumbers less than 1700 cm⁻¹.

C-H Vibrations

The FT-IR spectra of the heteroatomic structures show the presence of C-H stretching vibrations in the region of 3100-3000 cm⁻¹ [23], which is the characteristic region for the recognition of C-H stretching vibrations. In this region, bands are not considerably affected by the nature of the substituents. In the FT-IR spectrum of *N*-acetylisatin, bands were observed at 3130, 3072, 2972, 2994 and 2939 cm⁻¹.

The FT-Raman modes are located in the range of 3215-3010 cm⁻¹ with the B3LYP/6-311++G(d,p) method with a PED contribution of above 96%. As expected these modes are stretching modes, as is evident from the PED column in Table 2. FT-Raman bands were identified experimentally at 3130, 3082, 3054, 3021, 2995 and 2940 cm⁻¹ due to C-H stretching vibrations.

The C-H in-plane and out-of-plane bending vibrations are normally present as a number of strong sharp bands in the regions of 1300-1000 and 1000-750 cm⁻¹, respectively [24]. In the present work, the in-plane bending vibrations are observed at 1376, 1334, 1306, 1210, 1163, 1112, 1094, 1039 and 1012 cm⁻¹ in the FT-IR spectrum and at 1379, 1334, 1307, 1263, 1215, 1172, 1152, 1100, 1042 and 1017 cm⁻¹ in the FT-

Raman spectrum. The theoretically computed frequencies for C-H vibrations by the B3LYP/6-311++G(d,p) method showed good agreement with the recorded spectra of the title molecule.

C=O and C-O Vibrations

The carbonyl bands are one of the most characteristic bands in IR spectra. Both the carbon and oxygen atoms of the carbonyl group move during bond vibration and they have nearly equal amplitudes. The carbonyl group is highly polar and therefore gives rise to an intense IR absorption band. The carbonyl frequencies can be altered by inter-molecular hydrogen bonding. The carbonyl band is reasonably easy to recognize due to its high intensity. However, it might overlap with other bands that are caused by aromatic vibrations meaning that their undisputed assignment is often difficult. A great deal of structural information can be derived from the exact position of the carbonyl group vibrations, which occur in the region of 1800-1700 cm⁻¹ [25]. Also, Ibrahim *et al.* documented that the C=O stretching vibration occurs at 1768-1614 cm⁻¹ and

they have assigned a strong FT-IR band at 1703 cm⁻¹ to be for a carboxyl C=O stretching vibration [26].

The C=O vibration bands in the FT-IR spectrum were observed at 1782 cm⁻¹ for the ketone carbonyl (C3-O11), at 1751 cm⁻¹ for the lactam carbonyl (C2-O10) and at 1711 cm⁻¹ for the amide carbonyl (C12-O13) and they occurred at 1781, 1759 and 1704 cm⁻¹ in its FT-Raman spectrum, respectively, with an 85% PED contribution. The calculated C=O vibration bands using B3LYP are in agreement with the experimentally determined bands in the FT-IR and FT-Raman spectra of the title compound and they are in accordance with the reported values [25, 26]

C-C Vibrations

The bands between 1650 and 1400 cm⁻¹ in aromatic and heteroatomic compounds are assigned to carbon vibrations [27]. The actual positions are determined not by the nature of the substituents, but rather by the form of the substitution around the aromatic ring. The C-C stretching vibrations of N-acetylisatin were observed at 1592 and 1460 cm⁻¹ in the FT-IR spectrum. In the FT-Raman spectrum, the vibrations were observed at 1610, 1592 and 1476 cm⁻¹. Torsion CCCC, NCCC, ONCC and OCCC vibrations are presented in Table 2. The theoretically scaled vibrations also showed good agreement with the experimentally recorded data.

C-N Vibrations

The identification of C=N and C-N vibrations is a very difficult task, since the mixing of several modes is possible in this region [28]. The C-N stretching vibrations were observed at 1267 and 909 cm⁻¹ in the FT-IR spectrum. In the FT-Raman spectrum, the vibrations were observed at 1263 and 930 cm⁻¹. The theoretically scaled wave vibrations showed good agreement with the experimental data.

3.3 Natural bond orbital (NBO) analysis

NBO analysis provides the most accurate possible 'natural Lewis structure' picture of φ , because all orbital details are mathematically chosen to include the highest possible percentage of electron density. A useful aspect of the NBO method is that it gives information about interactions in both filled and virtual orbital spaces, which can enhance the analysis of intra- and inter-molecular interactions. The second Fock matrix was carried out to evaluate

donor-acceptor interactions in the NBO analysis [29]. The interaction results in a loss of occupancy from the localized NBO of the idealized Lewis structure into an empty non-Lewis orbital. For each donor (i) and acceptor (i), the stabilization energy, E^2 , associated with the delocalization, $i \rightarrow j$, is estimated as:

$$E^{2} = \Delta E_{ij} = q_{i} \frac{F(i, j)^{2}}{(\varepsilon_{i} - \varepsilon_{i})}$$
(1)

where q_i is the donor orbital frequency, ε_i and ε_i are diagonal elements and F(i, j) is the off diagonal NBO Fock matrix element.

NBO analysis provides an efficient method for studying intra- and inter-molecular binding and interactions between bonds and also provides a convenient basis for investigating charge transfer and conjugative interactions in molecular systems. Electron donor orbitals, acceptor orbitals and interacting stabilization energy, resulting from the second order micro-disturbance theory, were reported. The more intensive interaction between the electron donors and acceptors, i.e. more donating tendency from the electron donors to the electron acceptors, lead to a greater extent of conjugation in the whole system. Delocalization of the electron density between occupied Lewis-type (bond or lone pair) NBO orbitals and formally unoccupied (anti-bonding or Rydberg) non Lewis NBO orbitals corresponds to a stabilising donor-acceptor interaction. NBO analysis has been performed on the *N*-acetylisatin at the B3LYP/6-311++G(d,p) level in order to elucidate the intra-molecular re-hybridization and electron density delocalization within the molecule. The intramolecular hyperconjugative interactions were formed by orbital overlap between σ and π (N-C, C-C, C-O and C-H) as well as between σ^* and π^* (N-C, C-C, C-O and C-H) bond orbitals, which results in an intra-molecular charge transfer, which stabilizes the system. These interactions were observed as an increase in electron density (ED) in the (N-C, C-C, C-O and C-H) anti-bonding orbitals, which weakened the respective bonds. The strong intra-molecular hyperconjugative interaction of the σ and π electrons of N-C, C-C, C-O and C-H to the N-C, C-C, C-O and C-H bonds of the ring led to the stabilization of some parts of the ring, as shown in Table S1. For example, the intra-molecular hyperconjugative interaction of N1-C2 distributes to σ*(N1-C9, N1-C12, C3-O11, C4-C9, C8-C9 and C12-C13) leading to a stabilization of 4.68 KJ/mol. This enhanced conjugation in the π bonding orbital (C7-C8) distributes to π^* (C4-C9 and C5-C6) which leads to strong delocalization of 27.43 and 17.65 KJ/mol, respectively. The same kind of interactions have been calculated in the C3-O11, C4-C9, C5-C6 and C12-C13 bonds, as shown in Table S1. The stabilization energies associated with the hyperconjugative interactions, LP(1) O10-(C2-O10) and LP(1)-(N1-C2), are found to be 1.36 and 2.59 KJ/mol, respectively, as shown in Table S1, which act to extend the inter-molecular hydrogen bonding. The most important interaction energies, related to the resonance in the molecule, result from electron donation from the bonding donors, σ (C14-H19) and σ (C12-C14), to the bonding acceptor, σ *(C14-H21), with stabilization energies of 10.88 and 4.14 KJ/mol calculated, respectively.

3.4 Non Linear Optical (NLO) Effects

Non linear optical (NLO) effects arise from the interaction of electromagnetic fields in various media, which produces new fields with altered phase, frequency, amplitude or other propagation characteristics [30]. The first order hyperpolarizability (β_{α}) and related properties (β_{α} , α_{α} and $\Delta\alpha$) of *N*-acetylisatin are calculated using the B3LYP/6-311++G(d,p) method based on the finite field approach. In the presence of an applied electric field, the energy of a system is a function of the electric field. First order hyperpolarizability is a third rank tensor that can be described using 3x3x3 matrices. The 27 components of the 3D matrix can be reduced to 10 components according to Kleinman symmetry [30]. These can be given in the lower tetrahedral format, as it is obvious that the lower parts of the 3x3x3 matrices are tetrahedral. The components of β are defined as the coefficients of a Taylor series expansion of the energy in an external electric field. When the external electric field is weak and homogeneous, the expansion becomes:

$$E = E^{0} - \mu_{\alpha} F_{\alpha} - 1/2\alpha_{\alpha\beta} F_{\alpha} F_{\beta} - 1/6\beta_{\alpha\beta\gamma} F_{\alpha} F_{\beta} F_{\gamma} + ...$$
 (2)

where E^0 is the energy of the unperturbed molecules, F_{α} is the field at the origin and μ_{α} , $\alpha_{\alpha\beta}$ and $\beta_{\alpha\beta\Upsilon}$ are the components of the dipole moment, polarizability and first order hyperpolarizabilities, respectively. The total static dipole moment (μ), mean polarizability (α_0) anisotropy of the polarizability ($\Delta\alpha$) and mean first order hyperpolaraizability (β), using the x, y and z components, are defined as follows:

$$\mu = (\mu_x^2 + \mu_v^2 + \mu_z^2)^{1/2}$$
 (3)

$$\Delta \alpha = 2^{1/2} [(\alpha_{yy} - \alpha_{yy})^2 + (\alpha_{yy} - \alpha_{zz})^2 + (\alpha_{zz} - \alpha_{yy})^2 + 6\alpha_{yy}^2]^{1/2}$$
 (4)

$$\mu_{\text{tot}} = \mu_0 + \alpha_{ii} E_i + \beta_{iik} E_i E_k + \dots$$
 (5)

$$\alpha_{\text{tot}} = \frac{\alpha_{xx} + \alpha_{yy} + \alpha_{zz}}{3} \tag{6}$$

$$\beta_{tot} = \sqrt{\beta^2_x + \beta^2_y + \beta^2_z} \tag{7}$$

$$\beta tot = \sqrt{(\beta_{xxx} + \beta_{xyy} + \beta_{xzz})^2 + (\beta_{yyy} + \beta_{yzz} + \beta_{xxy})^2 + (\beta_{zzz} + \beta_{xxz} + \beta_{yyz})^2}$$
(8)

Since the values of the polarizabilities (α) and hyperpolarizabilities (β) from the Gaussian 03W output are reported in atomic units (a.u.), the calculated values have been converted into electrostatic units (esu). The dipole moment, first order hyperpolarizability and mean polarizability values are summarised in Table 3.

3.5 Analysis of the Molecular Electrostatic Potential (MEP)

The mapping of the electrostatic potential onto the isoelectron density surface simultaneously displays the electrostatic potential (electron + nuclei) distribution, molecular shape, size and dipole moments of the molecule and it provides a visual method for understanding the relative polarity [31]. The total electron density and MEP surfaces of the molecule under investigation are constructed using the B3LYP/6-311++G(d,p) method (Figure 5). The charges, derived from an electrostatic potential computation, gave useful information about chemical reactivity. The electrostatic potential was computed by creating an electrostatic potential grid. These atomic point charges gave a better indication of the likely sites of attack.

The color scheme for the MEP surface is red for electron rich and partial negative charge regions, blue for electron

Table 3: NLO properties of *N*-acetylisatin.

Parameters	B3LYP/6- 311++G(d,p)	Parameters	B3LYP/6- 311++G(d,p)
μ_{x}	-0.8611786	β _{xxxx}	481.3153837
μ_{y}	0.1380768	β_{xxxy}	-290.510381
μ_{z}	-0.000723	β_{xyy}	144.3399937
μ	0.872177613	β_{yyy}	175.098216
α_{xx}	171.4783121	β_{xxxz}	0.9276324
α_{xy}	-0.440524	β_{xyz}	-0.9537041
α_{yy}	147.4410319	β_{yyz}	-0.8289544
α_{yz}	-0.2775707	β_{xzz}	-63.9971074
α_{zz}	65.7509367	β_{yzz}	4.1019807
α_{tot}	1.9003X10 ⁻²³	β_{zzz}	-0.2532351
Δα(a.u)	312.136356	β_{tot}	572.581866
Δα(e.s.u)	4.6259X10 ⁻²³	$\beta_{tot}(e.s.u)$	4.9467X10 ⁻³⁰

deficient and partial positive charge regions, light blue for slightly electron deficient regions, vellow for slightly electron rich regions and green for neutral regions. The regions around the carbonyl groups (red) have the most negative potentials. The predominance of light green regions in the MEP surfaces corresponds to a potential balance between the two extremes, red and dark blue.

3.6 HOMO-LUMO Analysis

Both the highest occupied molecular orbitals (HOMO) and lowest unoccupied molecular orbitals (LUMO) play a role in the chemical stability of compounds [32]. The HOMO represents the ability to donate an electron, while the LUMO represents the ability to obtain an electron. The HOMO and LUMO energy values for N-acetylisatin, calculated by the B3LYP/6-311++G(d,p) method, are given in Table 4.

Molecular orbitals can provide insight into the nature of reactivity and some of the structural and physical properties of molecules. The electronic transition absorption corresponds to the transition from the ground state to the first excited state, and is mainly described by a one electron excitation from the HOMO to the LUMO [33]. The energy gap between the HOMO and LUMO has been used to prove bioactivity from intra-molecular charge transfer. The frontier molecular orbitals are mainly composed of p atomic orbitals, so electronic transitions from the HOMO to LUMO are mainly derived from the electronic transition of $\pi - \pi^*$. The energy gap demonstrates the kinetic stability of the molecules. A molecule with a small frontier orbital gap is more polarizable, which implies high chemical activity and low kinetic stability. The HOMO-LUMO energies and the orbital energy gaps for N-acetylisatin were calculated using the B3LYP/6-311++G(d,p) method and the pictorial representation of its frontier molecular orbitals is shown in Figure 6. The red and blue solid regions represent the molecular orbitals with completely opposite phases.

3.7 Local Reactivity Descriptors

The most relevant local descriptor of reactivity is the Fukui function, which is the derivative of the electronic chemical potential with respect to the external potential due to compensation of nuclear charges in the system. These reactivity indices are directly concerned with the selectivity of the molecule towards specific chemical events. The Fukui function of the system defines the more reactive regions in a molecule. Using Mulliken

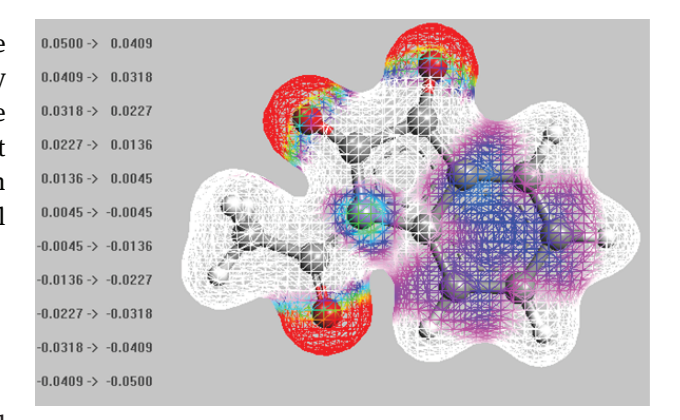


Figure 5: Molecular electrostatic potential map of N-acetylisatin calculated at B3LYP/6 311++G(d,p) level.

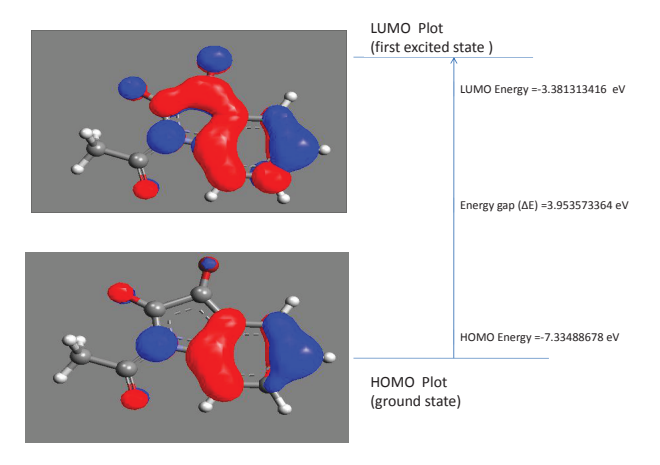


Figure 6: Frontier molecular orbitals of N-acetylisatin.

Table 4: HOMO-LUMO energies of N-acetylisatin.

Property	Energy
E _{HOMO} (eV)	-7.33488678
E _{LUMO} (eV)	-3.381313416
$\Delta E = E_{\text{max}} - E_{\text{max}} (eV)$	3.953573364

atomic charges of the neutral, cation and anion states of *N*-acetylisatin, Fukui functions $(f_{\nu}^{+}; f_{\nu}^{-}; f_{\nu}^{0})$, local softness $(s_{\nu}^{+}; s_{\nu}^{-}; s_{\nu}^{0})$ and local electrophilicity indices $(\omega_{\nu}^{+}; \omega_{\nu}^{-}; s_{\nu}^{0})$ ω_{ν}^{0}) are calculated [34, 35]. Fukui functions are calculated using the following equations:

$$f_{\nu}^{+} = [q(N+1) - q(N)]$$
 for nucleophilic attack (9)

$$f_{k} = [q(N) - q(N-1)]$$
 for electrophilic attack (10)

$$f_{\nu}^{0} = 1/2[q(N+1) - q(N-1)]$$
 for radical attack (11)

Local softness and electrophilicity indices are calculated using the following equations:

234 — Maha S. Almutairi et al.

Table 5: Mulliken population analysis, Fukui functions, local softness in eV, electrophilicity indices in eV for atoms of N-acetylisatin.

Atoms	Mulliken atomic charges		Fukui functions		Local softness		Electrophilicity indices					
	qn+1	qn	qn-1	fk+	fk-	fk0	sk+	sk-	sk0	ωk+	ωk-	ωk0
N1	0.1452	0.0527	0.0305	0.0925	0.0222	0.0573	0.0086	0.0021	0.0054	0.0337	0.0081	0.0209
C2	0.1456	0.1402	0.0523	0.0054	0.0879	0.0466	0.0005	0.0082	0.0044	0.0020	0.0320	0.0170
С3	-0.1448	-0.1767	-0.2875	0.0318	0.1108	0.0713	0.0030	0.0103	0.0067	0.0116	0.0404	0.0260
C4	0.5639	0.5518	0.5959	0.0121	-0.0442	-0.0160	0.0011	-0.0041	-0.0015	0.0044	-0.0161	-0.0058
C5	-0.1717	-0.2119	-0.2805	0.0402	0.0685	0.0544	0.0037	0.0064	0.0051	0.0147	0.0250	0.0198
C6	-0.5435	-0.6057	-0.562	0.0622	-0.0434	0.0094	0.0058	-0.0040	0.0009	0.0227	-0.0158	0.0034
C7	-0.1564	-0.1808	-0.2445	0.0244	0.0637	0.0440	0.0023	0.0059	0.0041	0.0089	0.0232	0.0161
C8	-0.0394	-0.0950	-0.1262	0.0556	0.0311	0.0434	0.0052	0.0029	0.0040	0.0203	0.0114	0.0158
C9	0.2438	0.2549	0.2620	-0.0111	-0.0070	-0.0091	-0.0010	-0.0007	-0.0008	-0.0041	-0.0026	-0.0033
010	-0.0631	-0.1595	-0.346	0.0964	0.1869	0.1417	0.0090	0.0174	0.0132	0.0352	0.0681	0.0517
011	-0.1785	-0.2801	-0.4640	0.1016	0.1839	0.1427	0.0095	0.0172	0.0133	0.0371	0.0670	0.0521
012	0.2261	0.2425	0.2445	-0.0164	-0.0021	-0.0092	-0.0015	-0.0002	-0.0009	-0.0060	-0.0008	-0.0034
013	-0.1780	-0.3103	-0.3690	0.1323	0.0588	0.0955	0.0123	0.0055	0.0089	0.0482	0.0214	0.0348
C14	-0.5621	-0.5806	-0.5865	0.0186	0.0059	0.0122	0.0017	0.0005	0.0011	0.0068	0.0021	0.0045
H15	0.2666	0.2062	0.1595	0.0604	0.0467	0.0535	0.0056	0.0044	0.0050	0.0220	0.0170	0.0195
H16	0.2424	0.1569	0.0944	0.0855	0.0626	0.0740	0.0080	0.0058	0.0069	0.0312	0.0228	0.0270
H17	0.2541	0.1854	0.1188	0.0687	0.0666	0.0677	0.0064	0.0062	0.0063	0.0250	0.0243	0.0247
H18	0.2981	0.2553	0.2176	0.0428	0.0376	0.0402	0.0040	0.0035	0.0038	0.0156	0.0137	0.0147
H19	0.2404	0.2031	0.1569	0.0373	0.0462	0.0418	0.0035	0.0043	0.0039	0.0136	0.0169	0.0152
H20	0.2059	0.1759	0.1672	0.0300	0.0087	0.0193	0.0028	0.0008	0.0018	0.0109	0.0032	0.0071
H21	0.2056	0.17590	0.1673	0.0297	0.0086	0.0192	0.0028	0.0008	0.0018	0.0108	0.0031	0.0070

$$S_{\nu}^{+} = S f_{\nu}^{+}, S_{\nu}^{-} = S f_{\nu}^{-}, S_{\nu}^{0} = S f_{\nu}^{0}$$
 (12)

$$\omega_{\nu}^{+} = \omega f_{\nu}^{+}, \ \omega_{\nu}^{-} = \omega f_{\nu}^{-}, \ \omega_{\nu}^{0} = \omega f_{\nu}^{0}$$
 (13)

where +, - and 0 show nucleophilic, electrophilic and radical attack, respectively.

Fukuifunctions, locals oftness and local electrophilicity indices for selected atomic sites in the title molecule are listed in Table 5. The maximum values of all three local electrophilic reactivity descriptors $(f_k^+; S_k^+; \omega_k^+)$ at atom H24 indicate that this site is prone to nucleophilic attack. In the same way, the maximum values of the nucleophilic reactivity descriptors $(f_k^-; S_k^-; \omega_k^-)$ at C6 indicate that this site is more prone to electrophilic attack [36].

3.8 Mulliken Population Analysis

Mulliken atomic charge calculation has an important role in the application of quantum chemical calculations to molecular systems because atomic charges affect the dipole moment, molecular polarizability, electronic structure and a number of other properties of molecular systems [31]. The charge distribution over the atoms suggest the formation of donor and acceptor pairs involving charge transfer in the molecule. The Mulliken population analysis of N-acetylisatin is calculated using B3LYP with the 6-311++G(d,p) basis set and is presented in Table 5. It is noteworthy that the C4 atom of the title compound exhibited more positive charge, whereas the C3, C5, C6, C7, C8, C10, C11, C13 and C14 atoms exhibited negative charges. The N1, C2, C4, C9, O12 and H15-H21 atoms exhibited only positive charges. The charge on H18 has the maximum magnitude of 0.29381 among the hydrogen atoms and C8 has the least magnitude in the molecule. However, H15-H21 atoms possess positive charge distributions due to the large negative charges on the carbon atoms. The charge distribution of *N*-acetylisatin is shown in Figure 7.

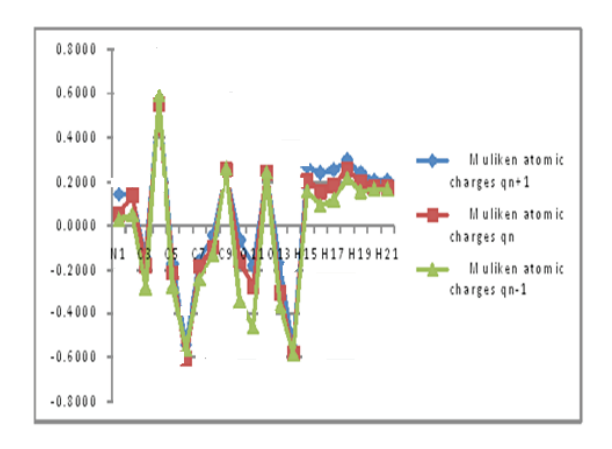


Figure 7: Mulliken population analysis of N-acetylisatin.

3.9 Thermodynamic Properties

The total energy of a molecule is the sum of the translational, rotational, vibrational and electronic energies, i.e. E = Et + Er + Ev + Ee. A statistical thermochemical analysis of N-acetylisatin was carried out with the assumption of room temperature and one atmospheric pressure. On the basis of vibrational analysis and statistical thermodynamics, the standard thermodynamic functions, heat capacity $(C^{\scriptscriptstyle 0}_{p,m})\text{, entropy }(S^{\scriptscriptstyle 0}_{m})\text{, and enthalpy }(H^{\scriptscriptstyle 0}_{m})$ were obtained and are listed in Table 6. $C^{o}_{p,m}$, $S^{o}_{p,m}$ and H^{o}_{m} all increased with increasing temperature from 100 to 1000 K. This might be attributed to the enhancement of the molecular vibration as a result of increasing temperature [37]. The corresponding fitting factors (R2) for these thermodynamic properties are 0.9996, 0.99996 and 0.99934, respectively. The correlation between these thermodynamic properties and temperature is shown in Figure 8 and the equations are given below:

$$C^{0}p,m = 14.96578 + 0.67679T -2.94375 X10^{-4}T^{2};$$
(R²= 0.9996) (14)

$$S^{0}m = 233.81496 + 0.75417T -1.86536 X10^{-4}T^{2};$$

(R²= 0.99996) (15)

$$H^{0}p,m = -8.29573 + 0.09023T + 1.76561 X10^{-4}T^{2};$$
 (R²= 0.99934) (16)

These equations could be used for further studies of N-acetylisatin. For instance, when we investigate the interaction between N-acetylisatin and another compound, the thermodynamic properties could be obtained from these equations and then used to calculate the change in the Gibbs free energy of the reaction, which will help us to judge the spontaneity of the reaction.

Table 6: Thermodynamic properties for *N*-acetylisatin obtained by B3LYP/6-311++G(d,p) method.

T (K)	S _m (J/mol.K)	C ^o _{p,m} (J/mol.K)	H ^o _{p,m} (kJ/mol)
100	305.48	81.53	5.52
200	378.58	135.88	16.38
298.15	442.87	189.43	32.36
300	444.04	190.41	32.71
400	505.83	240.4	54.31
500	564.14	282.39	80.52
600	618.74	316.33	110.52
700	669.63	343.64	143.56
800	717.01	365.84	179.07
900	761.19	384.1	216.6
1000	802.47	399.31	255.79

They can also be used to compute other thermodynamic functions and estimate the directions of chemical reactions according to the second law of thermodynamics. All thermodynamic calculations were performed for the gas phase. Scale factors have been recommended [38] for accurate prediction of the zero-point vibration energies, heat capacities, entropies and enthalpies.

3.10 NMR Spectral Analysis

Isotropic chemical shifts are frequently used as an aid for the identification of reactive organic species. It is recognized that accurate prediction of molecular geometry is essential for reliable calculations of Therefore, full magnetic properties. geometry optimization of N-acetylisatin was performed using the B3LYP/6-311++G(d,p) method. Then, Gauge-including atomic orbital 1H and 13C chemical shift calculations of *N*-acetylisatin were carried out using the same method. Such density functional methodologies offer an effective calculation method due to their low computational cost. The experimental and calculated NMR chemical shift values for N-acetylisatin are summarised in Table 7. The ¹H chemical shifts for *N*-acetylisatin were obtained by the complete analysis of its ¹H-NMR spectrum and interpreted critically in an attempt to understand the possible different effects acting on the shielding constants of the protons. The ¹H NMR spectrum was assigned according to the coupling pattern and constants. Additionally, the chemical shift value for C3 in N-acetylisatin was observed at higher value (180.16 ppm) than all other carbon atoms (26.45-169.71 ppm).

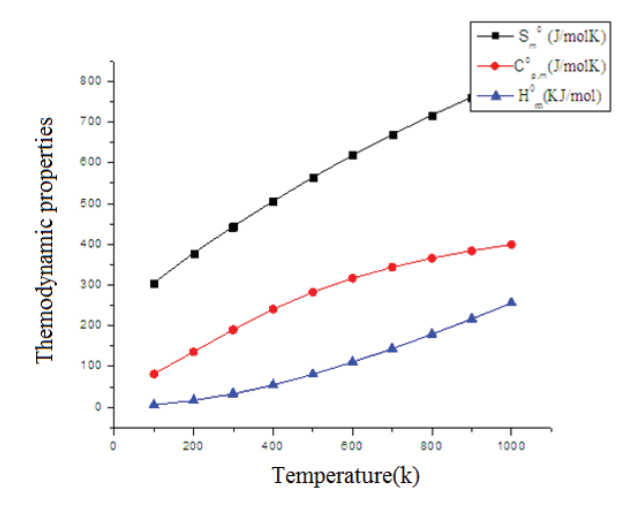


Figure 8: Correlation graphs of thermodynamic properties at different temperature of *N*-acetylisatin.

Table 7: Experimental and computed NMR (¹³C and ¹H) chemical shifts of t *N*-acetylisatin using B3LYP/6-311++G(d,p).

Atoms	Calculated	Experimental
Atoms	values (δ)	values (δ _{ics})
C2	163.90	157.96
C3	184.77	180.16
C4	117.29	118.24
C5	123.18	126.18
C6	119.47	125.27
C7	138.61	138.94
C8	110.28	119.20
C9	129.34	148.59
C12	163.31	169.71
C14	27.25	26.45
H15	7.37	7.77
H16	6.62	7.35
H17	7.28	7.71
H18	9.39	8.40
H19	2.54	2.73
H20	2.93	2.73
H21	2.94	2.73

4 Conclusions

In this investigation, the optimized molecular structure, thermodynamic, electronic, vibrational and spectroscopic properties of 1-acetyl-1*H*-indole-2,3-dione (*N*-acetylisatin) were calculated by DFT using the B3LYP/6-311++G(d,p) method. The optimized geometric parameters (bond lengths and angles) were theoretically determined by DFT and compared with the experimental values. Vibrational FT-IR and FT-Raman spectra were recorded. On the basis of agreement between the calculated and experimental results, the assignment of all fundamental

vibrational modes of N-acetylisatin was carried out based on the results of the PED output obtained from normal coordinate analysis. NBO analysis indicated the intramolecular charge transfer between the bonding and antibonding orbitals. In addition, the electric dipole moment, polarizabilities and the hyperpolarizabilities were calculated by the B3LYP/6-311++G(d,p) method. The MEP and HOMO-LUMO energy separation indicated the kinetic stability of *N*-acetylisatin. The HOMO-LUMO energy gap reflected the chemical activity of N-acetylisatin. Orbital energy interactions between selected functional groups were analyzed by the density of states. Fukui functions, local softness and electrophilicity indices for selected atomic sites in the title compound were calculated. Calculated and experimental NMR chemical shift values were also compared. In summary, the experimental data, along with the simulations, have allowed for the integrated characterization of N-acetylisatin.

Supplementary information: Figures S1 and S2 as well as Table S1 are provided as supporting information.

Acknowledgement: The authors would like to extend their sincere appreciation to the Deanship of Scientific Research at King Saud University for its funding of this research through the Research Group Project no. RGP-196.

References

- [1] Prenen H., Cools J., Mentens N., Folens C., Sciot R., Schöffski P., Van Oosterom A., Marynen P., Debiec-Rychter M., Efficacy of the kinase inhibitor SU11248 against gastrointestinal stromal tumor mutants refractory to imatinib mesylate, Clin. Cancer Res., 2006, 12, 2622–2627.
- [2] Motzer R.J., Michaelson M.D., Redman B.G., Hudes G.R., Wilding G., Figlin R.A., Ginsberg M.S., Kim S.T., Baum C.M., DePrimo S.E., Activity of SU11248, a multitargeted inhibitor of vascular endothelial growth factor receptor and plateletderived growth factor receptor, in patients with metastatic renal cell carcinoma, J. Clin. Oncol., 2006, 24, 16–24.
- [3] Daisley R.W., Shah V.K., Synthesis and antibacterial activity of some 5-nitro-3-phenyliminoindol-2-(3H)-ones and their N-Mannich bases, J. Pharm. Sci., 1984, 73, 407–408.
- [4] Varma R.S., Nobles W.L., Synthesis and antiviral and antibacterial activity of certain N-dialkylaminomethylisatin β-thiosemicarbazones, J. Med. Chem., 1967, 10, 972–974.
- [5] Piscopo E., Diurno M., Gagliardi R., Cucciniello M., Veneruso G., Studies on heterocyclic compounds: indol-2,3-dione derivatives. VII. Variously substituted hydrazones with antimicrobial activity, Bol. Soc. Ital. Biol. Sper., 1987, 63, 827–832.
- [6] Pandeya S., Sriram D., Nath G., De Clercq E., Synthesis, antibacterial, antifungal and anti-HIV activities of Schiff and

- Mannich bases derived from isatin derivatives and N-[4-(4'chlorophenyl)thiazol-2-yl]thiosemicarbazide, Eur. J. Pharm. Sci., 1999, 9, 25-31.
- [7] Pandeya S.N., Sriram D., Nath G., De Clercq E., Synthesis, antibacterial, antifungal and anti-HIV evaluation of Schiff and Mannich bases of isatin and its derivatives with triazole, Arzneim-Forsch., 2000, 50, 55-59.
- [8] Bhattacharya S., Chakrabarti A., Dose-related proconvulsant and anticonvulsant activity of isatin, a putative biological factor, in rats, Indian J. Exp. Biol., 1998, 36, 118-121.
- [9] Scott M.K., Baxter E.W., Bennett D.J., Boyd R.E., Blum P.S., Codd E.E., Kukla M.J., Malloy E., Maryanoff B.E., Piperazinylalkyl heterocycles as potential antipsychotic agents, J. Med. Chem., 1995, 38, 4198-4210.
- [10] Perni R.B., Farmer L.J., Cottrell K.M., Court J.J., Courtney L.F., Deininger D.D., Gates C.A., Harbeson S.L., Kim J.L., Lin C., Inhibitors of hepatitis C virus NS3· 4A protease. Part 3: P 2 proline variants, Bioorg. Med. Chem. Lett., 2004, 14, 1939-
- [11] James D.A., Koya K., Li H., Liang G., Xia Z., Ying W., Wu Y., Sun L., Indole-and indolizine-glyoxylamides displaying cytotoxicity against multidrug resistant cancer cell lines, Bioorg. Med. Chem. Lett., 2008, 18, 1784-1787.
- [12] Xu P., Lin W., Zou X., Synthesis of a peptidomimetic HCMV protease inhibitor library, Synthesis, 2002, 2002, 1017-1026.
- [13] Chen J., Cunico R.F., Synthesis of α -ketoamides from a carbamoylsilane and acid chlorides, J. Org. Chem., 2004, 69, 5509-5511.
- [14] Lamberth C., Jeanguenat A., Cederbaum F., De Mesmaeker A., Zeller M., Kempf H.-J., Zeun R., Multicomponent reactions in fungicide research: The discovery of mandipropamid, Bioorg. Med. Chem., 2008, 16, 1531-1545.
- [15] Chen Y.-H., Zhang Y.-H., Zhang H.-J., Liu D.-Z., Gu M., Li J.-Y., Wu F., Zhu X.-Z., Li J., Nan F.-J., Design, synthesis, and biological evaluation of isoquinoline-1, 3, 4-trione derivatives as potent caspase-3 inhibitors, J. Med. Chem., 2006, 49, 1613-1623.
- [16] Boechat N., Kover W.B., Bastos M.M., Romeiro N.C., Silva A.S.C., Santos F.C., Valverde A.L., Azevedo M.L.G., Wollinger W., Souza T.M.L., Oliveira de Souza S. L., de Frugulhetti I.C.P.P., Design, synthesis, and biological evaluation of new 3-hydroxy-2-oxo-3-trifluoromethylindole as potential HIV-1 reverse transcriptase inhibitors, Med. Chem. Res., 2007, 15, 492-510.
- [17] Frisch M.J., Trucks G.W., Schlegel H.B., Scuseria G.E., Robb M.A., Cheeseman J.R., Jr. Montgomery J.A., Vreven T., Kudin K.N., Burant J.C., et al., Gaussion 03 Program; Gaussian, Inc.: Wallingford, CT, USA, 2004.
- [18] Lee C., Yang W., Parr R.G., Development of the Colle-Salvetti correlation-energy formula into a functional of the electron density, Phys. Rev. B, 1988, 37, 785-789.
- [19] Dennington R.I., Keith T., Millam J., Eppinnett K., Hovell W., Gilliland R., Gauss View Version 3.09; Semichem, Inc.: Shawnee Mission, KS, USA, 2003.
- [20] Jamroz M.H., Vibrational energy distribution analysis, VEDA 4 program, Warasaw, Poland, 2004.
- [21] Zukerman-Schpector J., Castellano E., Pinto A.D.C., Da Silva J., Barcellos M., Structure of 1-acetylindole-2, 3-dione. Acta cryst. C: Cryst. Struct. Commun., 1992, 48, 760-762.
- [22] Muthu S., Ramachandran G., Paulraj E.I., Swaminathan T., Quantum mechanical study of the structure and spectroscopic (FT-IR, FT-Raman), first-order hyperpolarizability and NBO

- analysis of 1,2-benzoxazol-3-ylmenthane sulfonamide, Spectrochim. Acta A, 2014, 128, 603-613.
- [23] Arivazhagan M., Sambathkumar K., Jeyavijayan S., Density functional theory study of FT-IR and FT-Raman spectra of 7-acetoxy-4-methyl coumarin, Indian J. Pure Appl. Phys., 2010, 48, 716-722.
- [24] Sundaraganesan N., Saleem H., Mohan S., Ramalingam M., Sethuraman V., FT-IR, FT-Raman spectra and ab initio DFT vibrational analysis of 2-bromo-4-methyl-phenylamine, Spectrochim. Acta A, 2005, 62, 740-751.
- [25] Snehalatha M., Ravikumar C., Joe I.H., Jayakumar V., Vibrational spectra and scaled quantum chemical studies of the structure of Martius yellow sodium salt monohydrate, J. Raman Spectrosc., 2009, 40, 1121-1126.
- [26] Ibrahim M., Nada A., Kamal D.E., Density functional theory and FT-IR spectroscopic study of carboxyl group, Indian J. Pure Appl. Phys., 2005, 43, 911-917.
- [27] Varsanyi G., Vibrational spectra of seven hundred benzene derivatives, Academic press, NewYork, 1969.
- [28] Silverstein M., Basseler G.C., Morill C., Spectrometric identification of organic compounds, Wiley, New York, 1981.
- [29] Raj R.K., Gunasekaran S., Gnanasambandan T., Seshadri S., Structural, Spectroscopic (FT-IR, FT-Raman & UV-Vis) and theoretical studies of 4,6-dichloro-3-formyl coumarin, Int. J. Curr. Res. Aca. Rev., 2015, 3, 130-149.
- [30] Kleinman D., Nonlinear dielectric polarization in optical media, Phys. Rev., 1962, 126, 1977-1979.
- [31] Govindarajan M., Abdelhameed, A.S. Al-Saadi A.A., Attia M.I., Experimental and theoretical studies of the vibrational and electronic properties of (2E)-2-[3-(1H-imidazol-1-yl)-1phenyl-propylidene]-N-phenylhydrazinecarboxamide: An anticonvulsant agent, Appl. Sci., 2015, 5, 955-972.
- [32] Gunasekaran S., Balaji R.A., Kumaresan S., Anand G., Srinivasan S., Experimental and theoretical investigations of spectroscopic properties of N-acetyl-5-methoxytryptamine, Can. J. Anal. Sci. Spectrosc., 2008, 53, 149-162.
- [33] Magdaline J.D., Chithambarathanu T., FT-IR, FT-Raman and DFT investigation, NBO analysis, HOMO and LUMO analysis of 2-furoyl chloride, Int. J. Chemtech. Res., 2015, 8, 362-371.
- [34] Padmanabhan J., Parthasarathi R., Subramanian V., Chattaraj P., Electrophilicity-based charge transfer descriptor, J. Phys. Chem. A, 2007, 111, 1358-1361.
- [35] Geerlings P., De Proft F., Langenaeker W., Conceptual density functional theory, Chem. Rev., 2003, 103, 1793-1874.
- [36] Sıdır İ., Sıdır Y.G., Kumalar M., Taşal E., Ab initio Hartree-Fock and density functional theory investigations on the conformational stability, molecular structure and vibrational spectra of 7-acetoxy-6-(2, 3-dibromopropyl)-4, 8-dimethylcoumarin molecule, J. Mol. Struct., 2010, 964,
- [37] Bopp F., Meixner J., Kestin J., Thermodynamics and statistical mechanics, Academic Press Inc. (London) Ltd., New York, 1967.
- [38] O'Boyle N.M., Tendorholt A.L., Langer K.M., Software news and updates cclib: A library for package-independent computational chemistry algorithms, J. Comput. Chem., 2008, 29, 839-845.